

Synthesis and Characterization of Modified Nanocellulose-Based Adsorbent for Removal of Cu²⁺ Ion Metal in Wastewater

Noorhaslin CHE SU^{1,a}, Ain Aqilah BASIRUN^{1,b},
Nor Shahroon HAMEED SULTAN^{1,c}, Devagi KANAKARAJU^{2,d} and
Cecilia Devi WILFRED^{1,3,e*}

¹Centre of Research in Ionic Liquid, Universiti Teknologi PETRONAS, Persiaran UTP, 32610 Seri Iskandar, Perak, Malaysia

²Faculty of Resource Science and Technology, Universiti Malaysia Sarawak, 94300 Kota Samarahan, Sarawak, Malaysia

³Fundamental and Applied Sciences Department, Universiti Teknologi PETRONAS, Persiaran UTP, 32610 Seri Iskandar, Perak, Malaysia

^ahaslincs@gmail.com, ^bainaqilahbasirun@gmail.com, ^cnorshahroon23@gmail.com,
^dkdevagi@unimas.my, ^ececili@utp.edu.my

Keywords: Nanocellulose, Cu (II), Magnetite, TiO₂

Abstract. The continuous release of heavy metal from various industrial activities has been recognized as one of the major causes contributing to water pollutant. Herein, a novel magnetite adsorbent consisting of nanocellulose (NC), magnetite nanoparticles (MNP) and titanium dioxide (TiO₂) have been prepared using hydrothermal method. The adsorbent material with adsorption, magnetic and photocatalytic properties has been successfully synthesized and used for Cu²⁺ removal from industrial wastewater. The magnetite adsorbent made up of nanocellulose from sago was characterized by X-ray diffraction (XRD), Fourier Transform Infrared Spectroscopy, (FTIR), field emission scanning electron microscope (FESEM) for physicochemical study. XRD demonstrating high crystallinity of nanocellulose and displays well crystallized anatase TiO₂. TiO₂ embedded on the surface on NC/MNP were clearly observed through FESEM. The photocatalytic efficiency of the adsorbent degradation of Cu was evaluated using atomic adsorption spectroscopy (AAS). The NC/MNP showed removal of 54.1% of Cu²⁺ metal. Increase of TiO₂ loading (800µl) facilitate Cu removal up to 96% after 120 minutes exposure under ultraviolet irradiation. Kinetic analysis using the PSO model at 100mg/L of Cu²⁺ gave a value of equilibrium adsorption capacity, q_e of 4.29 mg/g and a value of the pseudo-second-order rate constant, K_2 of 0.004 (95% C.I., 0.0037 to 0.012). The result from these studies showed that the combination of nanocellulose, magnetite and TiO₂ has potential heavy metal removals.

Introduction

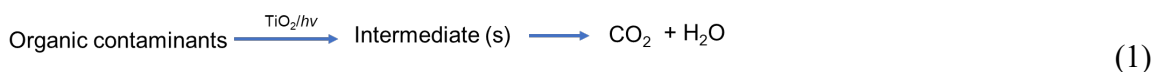
Rapid urbanization, industrialization and growing population have led a serious water pollution. Discharging untreated heavy metals such as Hg²⁺, Cu²⁺, Ni²⁺, and Cr⁷⁺ into river or sea can give band effect to human health and disturb the aquatic system. Cu²⁺ is one of the common heavy metals in wastewater originated from the effluents of electroplating, electrical industry, wire mills and other industrial plants. Accumulation of Cu²⁺ in human body above 1.3mg/L level enriched through the food chain for short period of time ions can cause mucosal irritation, intestinal problems widespread capillary and renal damage [1].

Nanocellulose (NC) based materials in recent years, which can offer promising results in wastewater purification [2]. The prospect of developing cellulose into nanocellulose by different physicochemical approaches has opened a new field for research into the advantages and possibilities of wastewater treatment. The enormous hydroxyl group (-OH) in nanocellulose can

efficiently anchor metal cations for heavy metal removal [3-5]. To effectively remove pollutants, NC has a remarkable explicit mechanical behaviour and chemically changed surface functioning that favoured the waste absorption [6]. On top of that, NC can be more cost-effective than other nanomaterials like graphene and ceramics owing to their low cost of the raw material and simple processing.

Several approaches have been reported for removing organic impurities from wastewater including the adsorption technique [7], membrane separation [8] and advanced oxidation process (AOP) [9] etc. Adsorption is the process by which a pollutant, such as organic compound and heavy metal ions are immobilized to the surface of a solid object by chemical or electrostatic in water treatment activity [10]. Magnetite (Fe₃O₄) nanoparticles have attracted scientific attention to be used as adsorbent due to their outstanding performance, such as their ability to display superparamagnetic properties with high saturation magnetization in the presence of external magnetic field [11]. Magnetite served with high surface area, good compatibility, low toxicity, and good physicochemical stability have been developed for potential application to detoxification of groundwater, surface water and industrial effluents in wastewater treatment [12].

Photocatalysis as part of the AOP process been extensively studied. Generally, photocatalysis consists of semiconductor structures. The most common semiconductor used for photocatalysis is TiO₂. As the TiO₂ semiconductor is illuminates by light, the TiO₂ gain equal or greater photon energy between VB and CB, the electron (e⁻) from valance band (VB) jump to conduction band (CB) and leave positively charged hole (h⁺) on VB. This pair of e⁻ and h⁺ can respectively migrate to the surface of the semiconductor to undergo series of oxidation and reduction which are embodied in the conversion of different valance states in the treatment of heavy metal. Photocatalysis also known as a “catalytic” reaction by adsorption of light which could mineralize organic compound into non-toxic product such as carbon dioxide and water [13] [14-16]. The possible mechanism occur during TiO₂ photocatalyst are shown in Eq. 1 [17].



This study will evaluate an adsorbent consisting of nanocellulose from sago, Fe₃O₄ and TiO₂ for synergistic interaction of adsorption and photocatalysis in removing Cu²⁺ from wastewater.

Materials and Method

Chemicals

Nanocellulose was obtained from sago bark and sago shell samples collected from Sarawak. Iron (III) hexahydrate (FeCl₃.6H₂O), iron (II) chloride tetrahydrate (FeCl₂.4H₂O), trisodium citrate (Na₃C₆H₅O₇) and sodium hydroxide (NaOH) from Merck (Germany). Titanium (IV) *n*-butoxide (TBOT) and ethanol were purchased from Merck.

Instrumentation

The powder phase compositions were identified with X-ray diffraction (XRD) equipment (D/max 2550 PC, Rigaku Co., Japan) using Cu K α radiation at 40Kv and 200mA. The functional groups of the nanocellulose adsorbents were determined using Fourier-transform infrared spectrophotometer (FTIR) instrument (Model Frontier, Thermo Fisher Scientific, Waltham, MA, USA). The morphology was observed by Field Emission Scanning Electron Microscope (FESEM) (Supra 55VP Carl Zeiss, Germany) equipped with an energy dispersive X-ray and field emission scanning electron microscope (Clara Tescan). The nitrogen adsorption and desorption isotherm were obtained at 77K using Autosorb -1 MP (Quantachrome, USA) utilizing Barret-Emmett-Teller calculations of pore volume and pore size (diameter) distributions from the desorption branch of

the isotherm. The concentration of Cu^{2+} ions was determined by an atomic absorption spectrometer (AAS) from Agilent (Model 240 FS, Agilent Technologies, United States). The non-linear regression of all kinetic models was plot and analysed using Curve Expert 6.0.

Preparation of nanocellulose

1 g of was extracted cellulose from sago was hydrolysed with 20 mL of acid and H_2SO_4 (40 wt.%) with ratio 1:20 at 45 °C for 60 min. The suspension was washed repeatedly using cold deionized water (centrifuge at 4000 rpm, 30 min) to remove the excess H_2SO_4 until pearl white with a neutral pH sedimentation were obtained. The slurry was further treated by sonication for 40 min in a sonicator before placing in a freezer-dryer. The nanocellulose powder was characterized by X-ray diffraction (XRD), infrared (FTIR, and field emission scanning electron microscopy (FESEM) analysis.

Preparation of nanocellulose/ Fe_3O_4

0.5 g nanocellulose was dissolved in 20ml of H_2O with vigorous mechanical stirring at 80 °C in a water bath until a homogenous solution was formed. Subsequently, 0.45 g Fe_3O_4 and 1.21 g of sodium acetate were added in a viscous solution of nanocellulose with vigorous agitating for 30 min at 80 °C in a water bath to form a homogeneous solution. Then, the solution was poured into a Teflon-lined stainless-steel autoclave for hydrothermal. Later cooling to ambient temperature, the black precipitate product was separated by a magnet and washed several times with water and ethanol. The as-prepared sample was dried overnight at 50 °C in the oven.

Preparation of nanocellulose/ $\text{Fe}_3\text{O}_4/\text{TiO}_2$

0.10 g nanocellulose/ Fe_3O_4 powder was added into 10 mL absolute ethanol solution and sonicated for ca. 20 min in an ultrasonic bath. 200 μL of TBOT was added into the dispersion dropwise, and the mixture was sonicated for 15 min. It was then decanted into a vapor phase hydrolysis apparatus (VPHA) with deionized water situated at the bottom of it to produce vapor at raised temperature. The closed VPHA was heated to 110°C and maintained for 5 hr. Then, the VPHA was cooled to room temperature. The as-prepared powder was collected by magnet and washed with absolute ethanol and deionized water and dried in the oven at 50 °C. Table 1 describes the two types of adsorbent prepared.

Table 1. Prepared adsorbent.

Adsorbent	Sample code
Nanocellulose/ Fe_3O_4	Ads-1
Nanocellulose/ $\text{Fe}_3\text{O}_4/\text{TiO}_2$	Ads-2

Photocatalytic reaction

The photocatalytic activity of adsorbent Ads-1 and Ads-2 was evaluated by activity of the adsorbent in terms of removal of Cu^{2+} in wastewater under UV-light illumination using 100-W UV lamp (UVP Co.Upland),Canada) at 365nm. Initial concentration of Cu^{2+} was 100mg/L. In the experiment, the suspension was stirred magnetically (200 rpm) at dark for 30 min. After 30 minutes in dark, 10 ml sample was taken from the wastewater by means of syringe filter. This method was repeated for 30, 60, 90 and 120 min under UV-light illumination. Collected samples were analysed with AAS to determine the concentration of Cu^{2+} . The Cu^{2+} removal was calculated by the following formula from the following Eq. 2 [12, 18].

$$R (\%) = [C_0 - C_1]/C_0 \times 100 \% \quad (2)$$

Where R is the removal percentage of Cu^{2+} ; and C_0 is the initial concentration of Cu^{2+} (mg/L); C_1 is the concentration of Cu^{2+} at reaction time (mg/L).

Results and Discussion

Physicochemical Study

Fig. 1 shows XRD peak for nanocellulose, Ads-1 and Ads-2. The nanocellulose shows the appearance peak at 15.28 and 22.94 [19]. The Ads-1 shows the appearance of the peak 22.94°, 30.06°, 35.76°, 43.5°, 57.11° and 62.5°. The peaks of nanocellulose 15.28° disappear with addition of Fe₂O₃ and the intensity of the nanocellulose peak at 22.94° were less for both Ads-1 and Ads-2 which, corresponds to the interaction of nanocellulose and magnetite. The dominate peaks were observed in both Ads-1 and Ads-2 at 30.06 °, 35.76°, 43.5°, 57.11 ° and 62.5° which, represents the present of Fe₃O₄ [11]. The Ads-2 shows similar peaks with Ads-1, with additional peaks observed at 25.26° and 54.3°. The peaks represent the anatase phase TiO₂ peak [20] which, demonstrates the formation of well-crystallized TiO₂.

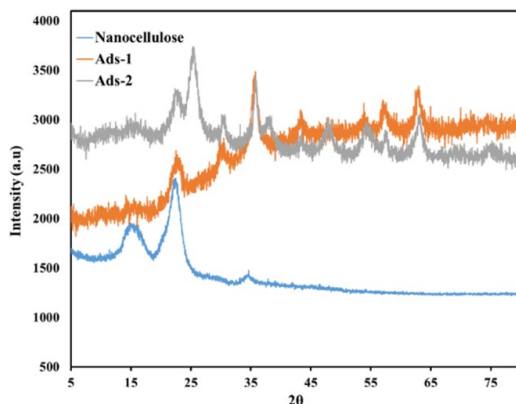


Fig. 1. XRD pattern of nanocellulose, Ads-1 and Ads-2.

Fig. 2 shows the FTIR spectra of the nanocellulose, Ads-1 and Ads-2. The wide absorption band at 3403 cm⁻¹ and 1645cm⁻¹ can be attributed to the stretching vibration of O-H from the hydroxyl group [21-22]. The absorption band at 2901 cm⁻¹ is associated with -C-H stretching vibrations [23]. The characteristic cellulose peak of pyranose ring was noticed at 1063 cm⁻¹[4]. Meanwhile, the high intensity band for iron oxide at 589 cm⁻¹ was found in the prepared Ads-1 and Ads-2 [22, 24]. This peak confirms the successful formation of Fe₃O₄ nanoparticles on the surface of nanocellulose.

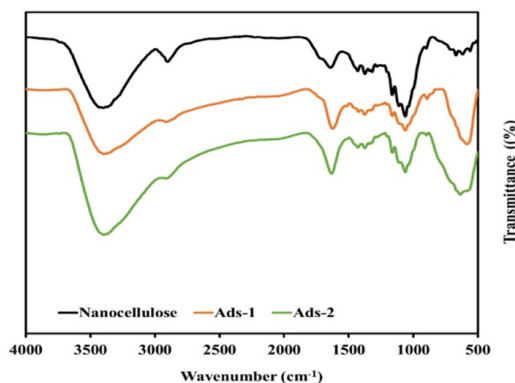


Fig. 2. FTIR spectra of nanocellulose, Ads-1 and Ads-2.

Fig. 3(a-d) shows the FESEM images of raw sago, treated sago with KOH and acid hydrolysis and the prepared adsorbent, respectively. From the figures, the morphology of the sago changes with each treatment. The smooth surface of raw sago is shown as in Fig. 3(a). The presence of a smooth surface represents the hemicellulose and lignin in the amorphous state [25]. The fibre

surface becomes rougher after being treated with KOH (Fig. 3(b)). This could indicate the partial removal of the outer non-cellulosic layer such as hemicelluloses, lignin, pectin, wax, and other impurities contained in sago [26-27]. Fig. 3(c) depicts the nanocellulose after acid hydrolysis. The acid hydrolysis breaks the fibres into nanoscale [28]. Fig. 3(d) represents the prepared adsorbent. White particle on Ads-2 surface was identified as TiO₂ particles. This finding shows that TiO₂ particles were well dispersed on the nanocellulose and magnetite surface.

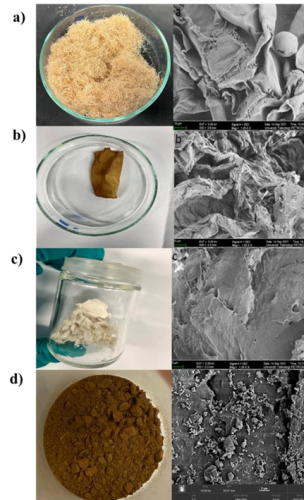


Fig. 3. FESEM images of (a) raw sago, (b) treated sago with KOH, (c) nanocellulose, and (d) prepared adsorbent.

The N₂ adsorption-desorption isotherm shown in Fig. 4 of adsorbent Ads-1 and Ads-2 presents a type-IV like curve with H3 hysteresis loop, characteristics of mesopores in the spherical cores and shells. The hysteresis loop of both Ads-1 and Ads-2 illustrates the fact that the larger crystallite stacking larger intraparticle pores at elevated temperature. Type IV isotherms show the cooperative adsorption where the binding site on the surface is identical, which can host multiple molecules. This applies to this present study since the adsorbent consists of nanocellulose and Fe₃O₄ components which provide high affinity to various adsorbates [29].

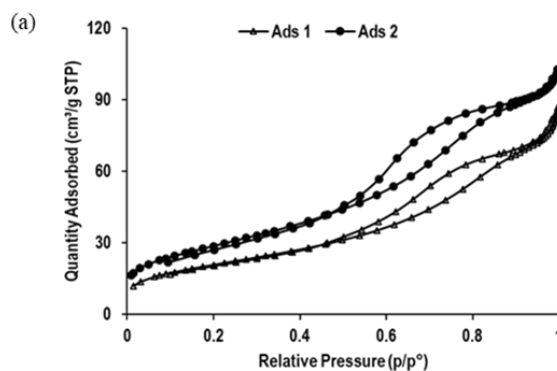


Fig. 4. N₂ Adsorption-desorption isotherm of Ads -1 and Ads-2.

Table 2 details the pore area and diameter of both prepared adsorbents. The average pore size of Ads-1 and Ads-2 are 6.853 nm and 6.011 nm, respectively. The pore diameter shows a decrement in value due to the agglomeration of TiO₂ which accumulates the surface of the adsorbent. The pore diameter of both samples show that adsorbent surface are mesopores. This data agrees with previous study which confirms that KOH modification of nanocellulose improves the porosity and enhance the affinity of the adsorbent towards pollutants.

Table 2. The results of BET analyses for the prepared adsorbents.

Adsorbent	BET surface area (m ² /g)	Pore diameter (nm)
Ads-1	74.87	6.853
Ads-2	103.39	6.011

Removal Studies of Cu²⁺ ion in wastewater

Fig. 5 compares the removal percentage of the prepared adsorbent. Ads-1 and Ads-2 showed Cu²⁺ removal of 54.1% and 96% respectively. The presence of nanocellulose and Fe₃O₄ in Ads-1 enables it to work as adsorbent to remove Cu²⁺ in wastewater. It is known that material with large amount amounts of active groups such as hydroxyl or carboxyl group in nanocellulose can absorb contaminants from wastewater [31]. As for Ads 2, there is a large improvement when TiO₂ is added to the adsorbent. TiO₂ has the ability of harvest light energy to stimulate the chemical reaction within the system. Heavy metal Cu²⁺ is removed almost completely from the wastewater. Table 3 displays previous studies where nanocellulose is used as adsorbent for heavy metal removal. Our work is comparable with the earlier work and shows that sago based nanocellulose + Fe₃O₄ + TiO₂ is a promising adsorbent in the near future.

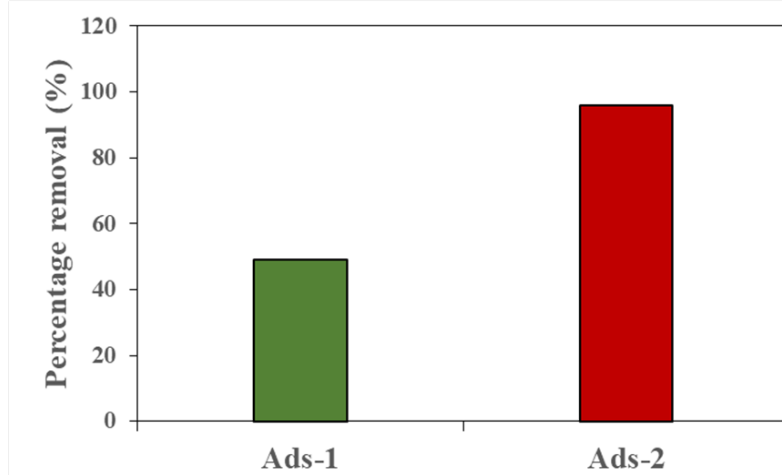


Fig. 5. Percentage of Cu²⁺ removal for Ads-1 and Ads-2.

Table 3. Comparative study of Cu²⁺ ion removal by different nanocellulose sources.

Nanocellulose sources	Metal ions (removal capacity)	References
Sago based NC + Fe ₃ O ₄ + TiO ₂	Cu ²⁺ (96 %)	This study
TEMPO-oxidized cellulose nanoparticles (TOCN)	Cu ²⁺ (75 mg/g)	[32]
Oryza sativa husk-NC	Cu ²⁺ (91 %)	[33]
Chitosan-NC	Cu ²⁺ (98 %)	[34]

Kinetic study

Kinetic models can provide information on adsorption pathways and the mechanisms that may be involved. This is also significant information for the process development and adsorption system design. Kinetics of 100 ppm Cu²⁺ removal using photocatalysis reaction is modelled using (a) pseudo-first order and (b) pseudo-second order a shown in Fig 6. The list of other error functions analysis is presented in Table 4 with pseudo-second order model giving the best values with the lowest AICc, RSME values of 0.56, 0.53, respectively and highest correlation coefficient, R² of 0.99, with bias and accuracy factors near unity. The pseudo-second order theory was

proposed by Blanchard et al. [35] and the derivation was developed by Azizian [36] assuming the initial adsorbate concentration is not too high as compared to the term derivation equation developed. Thus, the adsorption process obeyed the pseudo-second at lower initial Cu^{2+} concentration. In the pseudo-second order reaction, the rate-controlling step is linked to chemisorption. In this case, the adsorption mechanism is controlled chemically by the rate of adsorption. At low sorbate/sorbent ratios (first order at extremely low ratios), the sorption kinetics are often governed by a reversible second-order reaction, and at larger sorbate/sorbent ratios, the sorption kinetics are governed by two reversible second-order reactions that are competitive with one another. Kinetic analysis using the PSO model at 100mg/L of Cu^{2+} gave a value of equilibrium adsorption capacity, q_e of 4.29 mg/g and a value of the pseudo-second-order rate constant, K_2 of 0.004 (95% C.I., 0.0037 to 0.012) (Table 5).

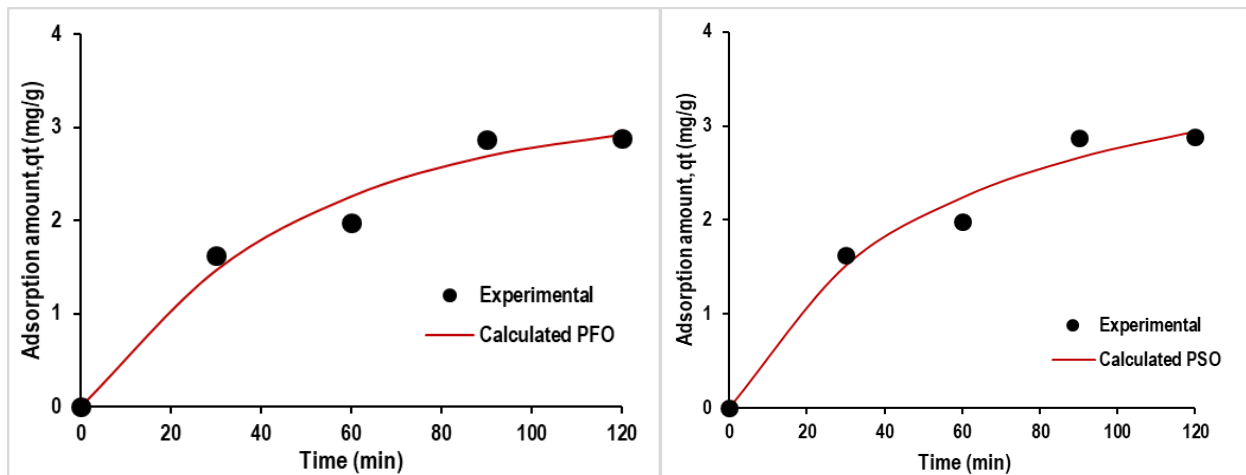


Fig. 6. Kinetics of 100 ppm Cu^{2+} removal using photocatalysis reaction as modelled using the (a) pseudo-first order and (b) pseudo-second order.

Table 4. Error function analysis of selective kinetics models.

Model	Parameter	SSE	R_2	AICc	AF	BF
Pseudo-1st order	2	0.229	0.990	-13.974	1.088	0.9994
Pseudo-2nd order	2	0.223	0.991	-14.243	1.034	0.9970

Table 5. Calculated maximum adsorption capacity of selective kinetic models and constant k for Cu^{2+} ion adsorption.

Model	Parameter	Maximum adsorption capacity, q_e (mg/g)	constant, k (95% confidence interval)
Pseudo-1st order	2	3.199	0.04 (0.023 to 0.05)
Pseudo-2nd order	2	4.291	0.004(0.0037 to 0.012)

Summary

In summary, this research has demonstrated that the synergistic interaction of adsorption and photocatalysis reaction for environmental purification is newly established and could be considered as one of the most efficient techniques. The result from these studies showed that the combination of nanocellulose, magnetite and TiO_2 has potential for heavy metal removals.

References

- [1] Q. Wu, N.F. Tam, J.Y. Leung, X. Zhou, J. Fu, B. Yao, L. Huang, Ecological risk and pollution history of heavy metals in Nansha mangrove, South China, *Ecotoxicology and Environmental Safety* 104 (2014) 143-151. <https://doi.org/10.1016/j.ecoenv.2014.02.017>
- [2] Y. Ahn, B.E. Logan, Effectiveness of domestic wastewater treatment using microbial fuel cells at ambient and mesophilic temperatures, *Bioresource Technology* 101 (2010) 469-475. <https://doi.org/10.1016/j.biortech.2009.07.039>
- [3] C.N.C. Hitam, A.A. Jalil, Recent advances on nanocellulose biomaterials for environmental health photoremediation: An overview, *Environmental Research* 204 (2022) 111964. <https://doi.org/10.1016/j.envres.2021.111964>
- [4] L.T. Yogarathinam, P.S. Goh, A.F. Ismail, A. Gangasalam, N.A. Ahmad, A.Samavati, S.C. Mamah, M.N.Z. Abidin, N.C. Ng, B. Gopal, Nanocrystalline cellulose incorporated biopolymer tailored polyethersulfone mixed matrix membranes for efficient treatment of produced water, *Chemosphere* 293 (2022) 133561. <https://doi.org/10.1016/j.chemosphere.2022.133561>
- [5] F. Asempour, D. Emadzadeh, T. Matsuura, B. Kruczek, Synthesis and characterization of novel Cellulose Nanocrystals-based Thin Film Nanocomposite membranes for reverse osmosis applications, *Desalination* 439 (2018) 179-187. <https://doi.org/10.1016/j.desal.2018.04.009>
- [6] T.K. Das, A. Poater, Review on the use of heavy metal deposits from water treatment waste towards catalytic chemical syntheses, *International Journal of Molecular Sciences* 22 (2021) 13383. <https://doi.org/10.3390/ijms222413383>
- [7] G. Lofrano, M. Carotenuto, G. Libralato, R.F. Domingos, A. Markus, L. Dini, R.K. Gautam, D. Baldantoni, M. Rossi, S.K. Sharma, M.C. Chattopadhyaya, M. Giugni, S. Meric, S. Polymer functionalized nanocomposites for metals removal from water and wastewater: an overview, *Water Research* 92 (2016) 22-37. <https://doi.org/10.1016/j.watres.2016.01.033>
- [8] M.S. Denny Jr, S.M. Cohen, *In situ* modification of metal-organic frameworks in mixed-matrix membranes, *Angewandte Chemie International Edition* 54 (2015) 9029-9032. <https://doi.org/10.1002/anie.201504077>
- [9] D. Kanakaraju, Y.C. Lim, A. Pace, Magnetic hybrid TiO₂/Alg/FeNPs triads for the efficient removal of methylene blue from water, *Sustainable Chemistry and Pharmacy* 8 (2018) 50-62. <https://doi.org/10.1016/j.scp.2018.02.001>
- [10] A. Mautner, Nanocellulose water treatment membranes and filters: a review, *Polymer International* 69 (2020) 741-751. <https://doi.org/10.1002/pi.5993>
- [11] J. Chang, Q. Zhang, Y. Liu, Y. Shi, Z. Qin, Preparation of Fe₃O₄/TiO₂ magnetic photocatalyst for photocatalytic degradation of phenol, *Journal of Materials Science: Materials in Electronics* 29 (2018) 8258-8266. <https://doi.org/10.1007/s10854-018-8832-7>
- [12] H.S. Hassan, M.F. Elkady, A.A. Farghali, A.M. Salem, A.I. Abd El-Hamid, Fabrication of novel magnetic zinc oxide cellulose acetate hybrid nano-fiber to be utilized for phenol decontamination, *Journal of the Taiwan Institute of Chemical Engineers* 78 (2017) 307-316. <https://doi.org/10.1016/j.jtice.2017.06.021>
- [13] R.L. Narayana, M. Matheswaran, A. Abd Aziz, Saravanan, P. Photocatalytic decolourization of basic green dye by pure and Fe, Co doped TiO₂ under daylight illumination, *Desalination* 269 (2011) 249-253. <https://doi.org/10.1016/j.desal.2010.11.007>

- [14] Y. Ku, I.L. Jung, Photocatalytic reduction of Cr (VI) in aqueous solutions by UV irradiation with the presence of titanium dioxide, *Water Research* 35 (2001) 135-142.
[https://doi.org/10.1016/S0043-1354\(00\)00098-1](https://doi.org/10.1016/S0043-1354(00)00098-1)
- [15] M.J. López-Muñoz, J. Aguado, A. Arencibia, R. Pascual, Mercury removal from aqueous solutions of HgCl₂ by heterogeneous photocatalysis with TiO₂, *Applied Catalysis B: Environmental* 104 (2011) 220-228. <https://doi.org/10.1016/j.apcatb.2011.03.029>
- [16] K.M. Joshi, B.N. Patil, D.S. Shirsath, V.S. Shrivastava, Photocatalytic removal of Ni (II) and Cu (II) by using different Semiconducting materials, *Advances in Applied Science Research* 2 (2011) 445-54.
- [17] M.N. Chong, B. Jin, C.W. Chow, C. Saint, Recent developments in photocatalytic water treatment technology: a review, *Water Research* 44 (2010) 2997-3027.
<https://doi.org/10.1016/j.watres.2010.02.039>
- [18] Q. Sun, H. Li, B. Niu, X. Hu, C. Xu, S. Zheng, Nano-TiO₂ immobilized on diatomite: characterization and photocatalytic reactivity for Cu²⁺ removal from aqueous solution, *Procedia Engineering* 102 (2015) 1935-1943. <https://doi.org/10.1016/j.proeng.2015.01.334>
- [19] S. Naduparambath, E. Purushothaman, Sago seed shell: determination of the composition and isolation of microcrystalline cellulose (MCC), *Cellulose* 23 (2016) 1803-1812.
<https://doi.org/10.1007/s10570-016-0904-3>
- [20] H. Zhang, X. He, W. Zhao, Y. Peng, D. Sun, H. Li, X. Wang, Preparation of Fe₃O₄/TiO₂ magnetic mesoporous composites for photocatalytic degradation of organic pollutants, *Water Science and Technology* 75 (2017) 1523-1528. <https://doi.org/10.2166/wst.2017.002>
- [21] S.B. Hammouda, N. Adhoum, L. Monser, Synthesis of magnetic alginate beads based on Fe₃O₄ nanoparticles for the removal of 3-methylindole from aqueous solution using Fenton process, *Journal of Hazardous Materials* 294 (2015) 128-136.
<https://doi.org/10.1016/j.jhazmat.2015.03.068>
- [22] N. Amiralian, M. Mustapic, M.S.A. Hossain, C. Wang, M. Konarova, J. Tang, J. Na, A. Khan, A. Rowan, Magnetic nanocellulose: A potential material for removal of dye from water, *Journal of Hazardous Materials* 394 (2020) 122571. <https://doi.org/10.1016/j.jhazmat.2020.122571>
- [23] I.J.D. Ebenezer, S. Ramalingam, C.R. Raja, P.J. Prabakar, Vibrational spectroscopic [IR and raman] analysis and computational investigation [NMR, UV-Visible, MEP and kubo gap] on L-Valinium picrate, *J. Nanotechnol. Adv. Mater* 2 (2014) 11-25. <https://doi.org/10.12785/jnam/020102>
- [24] V. Gopalakannan, N. Viswanathan, One pot synthesis of metal ion anchored alginate–gelatin binary biocomposite for efficient Cr (VI) removal, *International Journal of Biological Macromolecules* 83 (2016) 450-459. <https://doi.org/10.1016/j.ijbiomac.2015.10.010>
- [25] A.K. Veeramachineni, T. Sathasivam, S. Muniyandy, P. Janarthanan, S.J. Langford, L.Y. Yan, Optimizing extraction of cellulose and synthesizing pharmaceutical grade carboxymethyl sago cellulose from Malaysian sago pulp, *Applied Sciences* 6 (2016) 170.
<https://doi.org/10.3390/app6060170>
- [26] N. Yacob, M.R. Yusof, Z.M.A. Ainun, K.H. Badri, Effect of cellulose fiber from sago waste on properties of starch-based films, In *IOP Conference Series: Materials Science and Engineering* 368 (2018) 012028. <https://doi.org/10.1088/1757-899X/368/1/012028>
- [27] N.A. Rosli, I. Ahmad, I. Abdullah, Isolation and Characterization of Cellulose Nanocrystals from Agave angustifolia Fibre, *Bioresources* 8 (2013) 1893-1908

- [28] H. Kargarzadeh, I. Ahmad, I. Abdullah, A. Dufresne, S. Y. Zainudin, R.M. Sheltami, Effects of hydrolysis conditions on the morphology, crystallinity, and thermal stability of cellulose nanocrystals extracted from kenaf bast fibers, *Cellulose* 19 (2012) 855-866. <https://doi.10.1007/s10570-012-9684-6>
- [29] M.A. Al-Ghouti, D.A. Da'ana, Guidelines for the use and interpretation of adsorption isotherm models: A review, *Journal of Hazardous Materials* 393 (2020) 122383. <https://doi.10.1016/j.jhazmat.2020.122383>
- [30] S. Das, V.V. Goud, Characterization of a low-cost adsorbent derived from agro-waste for ranitidine removal, *Materials Science for Energy Technologies* 3 (2020) 879-888. <https://doi.10.1016/j.mset.2020.10.009>
- [31] A. Rahman, T. Urabe, N. Kishimoto, Color removal of reactive procion dyes by clay adsorbents, *Procedia Environmental Sciences* 17 (2013) 270-278. <https://doi.10.1016/j.proenv.2013.02.038>
- [32] X. Sun, X. Lv, C. Han., L. Bai, T. Wang, Y. Sun, Fabrication of Polyethyleneimine-Modified Nanocellulose/Magnetic Bentonite Composite as a Functional Biosorbent for Efficient Removal of Cu(II), *Water* 4 (2022) 2656. <https://doi.10.3390/w14172656>
- [33] M. Kaur, S. Kumari, P. Sharma, Removal of Pb (II) from aqueous solution using nanoadsorbent of *Oryza sativa* husk: Isotherm, kinetic and thermodynamic studies, *Biotechnology Reports* 25 (2020) e00410. <https://doi.10.1016/j.btre.2019.e00410>
- [34] Z. Ji, Y. Zhang, H. Wang, C. Li, Research progress in the removal of heavy metals by modified chitosan, *Tenside Surfactants Detergents* (2022) 2414. <https://doi.10.1515/tsd-2021-2414>
- [35] G. Blanchard, M. Maunaye, G. Martin, Removal of heavy metals from waters by means of natural zeolites, *Water research* 18 (1984) 1501-1507. [https://doi.10.1016/0043-1354\(84\)90124-6](https://doi.10.1016/0043-1354(84)90124-6)
- [36] S. Azizian, Kinetic models of sorption: a theoretical analysis. *Journal of colloid and Interface Science* 276 (2004) 47-52. <https://doi.10.1016/j.jcis.2004.03.048>